Rev.Adv.Mater.Sci. 13 (2006) 117-124

TRIBOLOGICAL STUDY OF NANO-MULTILAYERED ULTRA-HARD COATINGS BASED ON TiB_2

N. Panich[1], P. Wangyao[1], S. Hannongbua[1], P. Sricharoenchai[2] and Y. Sun[3]

[1]Metallurgy and Materials Science Research Institute, Chulalongkorn University, Phrayathai Rd., Pathumwan, Bangkok, 10330, Thailand
[2]Dept. of Metallurgical Engineering, Faculty of Engineering, Chulalongkorn University, Phrayathai Rd., Pathumwan, Bangkok, 10330, Thailand
[3]School of Engineering & Technology, De Montfort University, Leicester LE1 9BH, UK

Received: October 12, 2006

Abstract. In the present work, attempts have been made to fabricate the multilayered ultrahard coatings using sputtering technique, with the purpose to reduce the wear and to improve the tribological performance of the films for manufacturing applications. Several films have been produced by the use of direct current and radio frequency magnetron sputtering technique using titanium and TiB_2 as material targets and high speed steel as substrate. The resultant films were characterised by a variety of experimental and analytical techniques. Field emission scanning electron microscopy was used for film morphology and fractured cross-section examination. Nanoindentation was used to extract the intrinsic hardness and elastic modulus evaluation. Ball-on-disc sliding test under unlubricated sliding was employed for tribological measurement, for instance, friction coefficient and film wear-life.

The experimental results showed that the multilayered TiB_2 ultrahard coatings express high hardness and good coating adhesion. The enhanced adhesion is due to the technique of layering the hard layer with the tougher material as called multilayer structure. Under unlubricated sliding against an alumina ball, the TiB_2 multilayered ultrahard coatings produced under various deposition conditions increases the wear resistance of high speed steel by more than three times but extremely excellent wear resistance with encountering steel ball. It is noted that all samples can improve the wear resistance of high-speed steel. The multilayered TiB_2 ultrahard coatings provides a hard layer to resist plastic deformation and eliminate adhesion between the test surface and the ball slider, which are the main reasons of severe wear of untreated high speed steel.

1. INTRODUCTION

Titanium diboride (TiB_2) coatings have been attracting interest from industry due to its outstanding properties such as very high hardness, high chemical stability at high temperature and high wear resistance [1-3]. Although the structure and properties of deposited TiB_2 coatings have been studied by many investigators so far [4-7], one drawback of TiB_2 coatings is the poor adhesion to the substrate materials due to high compressive residual stress after deposition. It is well known that it is essential to control compressive stresses which develop during coating growth, since such stresses not only reduce coating adhesion but also limit film thickness. A possible way to obtain lower stress levels could be to utilise multilayer coatings, which involve the combination of the stressed material with a more ductile material in a layered structure [8]. Recently, in practice the uses of multilayer coatings offer suitable advantages when complimentary coating layers are chosen, for example, the use of alternate layers of ceramic and ductile materials to protect against erosion in gas turbine compressors [9] and the use in dry cutting application [10].

In this work, the multilayer systems have been proposed in order to overcome the problem of brittleness and the high residual stress of the TiB_2 coating deposited with stationary substrates by magne-

Corresponding author: P. Wangyao, e-mail: panyawat@hotmail.com

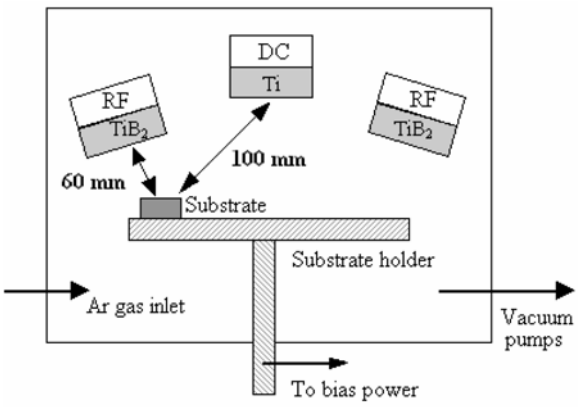

Fig. 1. The deposition set up in this study.

tron sputtering technique. Highly stressed TiB_2 coatings were layered with a ductile Ti. There are two reasons for choosing ductile Ti for multilayer structure. First, Ti has similar crystal structure (hcp) and chemistry to TiB_2, which shows the material compatibility. Second, Ti is mostly used to be an interlayer media between two materials owing to its strong adhesion to other materials. The multilayer coatings were deposited using magnetron sputtering with Ti and TiB_2 targets. To evaluate the coating phase composition X-ray diffraction was used. Mechanical properties were examined by nanoindentation for hardness and modulus and microscratch test for coating adhesion to substrate.

2. EXPERIMENTAL PROCEDURE

In this study, a commercial high-speed steel (HSS), SECO WKE45 (Sweden), in fully hardened and tempered condition was chosen as substrates. The specimen's surface was manually ground and polished. The HSS substrates were then ultrasonically cleaned with acetone and ethanol before charging the deposition chamber. A planar magnetron sputtering system supplied by the Coaxial Company (UK) was used for depositions. The system consists of a cylindrical chamber with three 3-in water cooled target holders tilted at approximately 30 degree with respect to the normal of the horizontal substrate holder, which can be heated by graphite heating elements. The substrates were positioned near to the edge of the working table below the TiB_2 target (see Fig. 1).

The substrates were stationary and the substrate-target distance was kept constant at 60 mm and 100 mm for TiB_2 and Ti targets, respectively. All the experiments were conducted at a constant working pressure of 0.65 Pa and at a total gas flow rate (Ar) of 20 sccm. The substrate temperature was 400 °C for all depositions. A RF power biased to the substrate was used to sputter clean the substrate surface for 90 min for all depositions. Both of DC and RF sputtering was used in this work by using DC power for the Ti target and RF power for the TiB_2 target as shown in Fig. 1. The DC and RF power employed in this study was 200 W for all depositions. Therefore, four types of TiB_2-based nanostructured coatings have been fabricated. These include:

(1) Graded Ti-TiB_2 coatings, by depositing a thin Ti interfacial layer at the interface followed by a TiB_2 layer on top,
(2) Multilayer Ti-TiB_2 coatings, by depositing 4 alternate Ti and TiB_2 layers with varying Ti layer thickness,
(3) Multilayer Ti-TiB_2 coatings, by depositing 6 alternate Ti and TiB_2 layers with varying Ti layer thickness.
(4) Multilayer Ti-TiB_2 coatings, by depositing 12 alternate Ti and TiB_2 layers with varying Ti layer thickness.

It is noted that the deposition time of TiB_2 was fixed in total of 3 h in all depositions. The details of deposition are summarized in Table 1.The phase composition of the resultant coatings was examined by Shimadzu X-ray diffractometer with Cu-K_α radiation. Chrystallographic phases were deduced by comparing the experimental diffraction patterns with the standard JCPDS data. The fractured cross-sections of the coatings were imaged using a field emission scanning electron microscope (FESEM), Joel JSM 6340F. The coating thickness was measured by making a ball-crater on the coating surface using the Calotest machine manufactured by CSEM, Switzerland. A stainless steel ball of 25.4 mm diameter was used for cratering with a speed of 700 rpm for 360 s. The roughness of surfaces was imaged using an atomic force microscopy (AFM), Digital Instrument.

Nanoindentation test was performed using the NanoTest™ instrument from Micro Materials Limited, the United Kingdom, with a Berkovich diamond indenter with the tip radius of 645 nm. All experiments were performed at a constant loading and unloading rate of 0.05 mN/s. In order to assess the intrinsic mechanical properties of the coatings i.e. hardness and modulus, all specimens were tested at 50 nm penetration depth to avoid any possible effect from the substrate during the indentation process. The unloading curves were used to derive the

Table 1. Deposition conditions.

Materials	Mode	Conditions
Sample 1	Graded Ti/TiB_2	Ti 20 min, TiB_2 3 h
Sample 2	Multilayer Ti/TiB_2	Ti 20 min, TiB_2 1.5 h & Ti 20 min, TiB_2 1.5 h
Sample 3	Multilayer Ti/TiB_2	Ti 20 min, TiB_2 1 h & Ti 20 min, TiB_2 1 h & Ti 20 min, TiB_2 1 h
Sample 4	Multilayer Ti/TiB_2	Ti 20 min, TiB_2 30 min & Ti 20 min, TiB_2 30 min & Ti 20 min, TiB_2 30 min & Ti 20 min, TiB_2 30 min & Ti 20 min, TiB_2 30 min & Ti 20 min, TiB_2 30 min

hardness and reduced modulus values by the analytical technique developed by Oliver and Pharr [11]. The reported hardness and modulus values are the average of 10 measurements.

The microscratch test was performed using the single-pass scratch mode available in the NanoTest™ device with a Rockwell diamond indenter topped with a conical with spherical end form of 25 mm in radius. The scanned length was scratched by applying a linearly increasing load at 5 mN/s after pre-scanning the initial 50 mm distance under a small initial load of 0.25 mN. During scratching, the friction force on the indenter and the surface profile along the full length of the scratched track were measured continually, such that a friction force versus scratching distance (or load) curve during-scratch profile were obtained. The critical load for coating failure (*Lc*), commonly used to measure of the coating-substrate adhesion strength, was determined by the sudden change in friction force, which also led to a sudden change in the profile.

The sliding wear behavior of the TiB_2 coated samples were investigated using a pin-on-disk tribometer (CSEM 15-208 Instruments, Neuchatel, Switzerland) in ambient atmosphere. An alumina ball of radius 3 mm was used as a counter face material against the films in this study because past research of dry sliding wear against stainless steel ball had shown that the stainless steel ball would wear out instead of the coating. This was further proven by the examination of the coating surface, where the ball's wear debris was found to have transferred to the coating surface. This finding may be

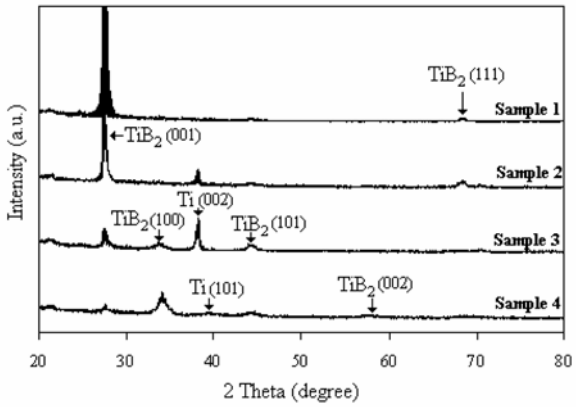

Fig. 2. XRD patterns of multilayer TiB_2 coatings.

explained by the fact that the stainless steel ball had lower hardness than the coated samples and thus lesser wear resistance. Hence the stainless steel ball would wear out more easily than the coated samples. This also proved that the coated samples had good wear resistance. Therefore, alumina ball was used in this project as it has higher hardness (18 GPa) and can more accurately display the actual wear behavior of the coated samples.

The linear speed and total sliding distance for all tests were fixed at 20 cm/s and 200 m respectively. Two types of sliding friction experiments were performed at ambient conditions and their conditions are stated below:

The surface topographical conditions of the wear tracks were then being analyzed under the SEM. The wear volume of the coated samples was then evaluated and analyzed using surface profiler.

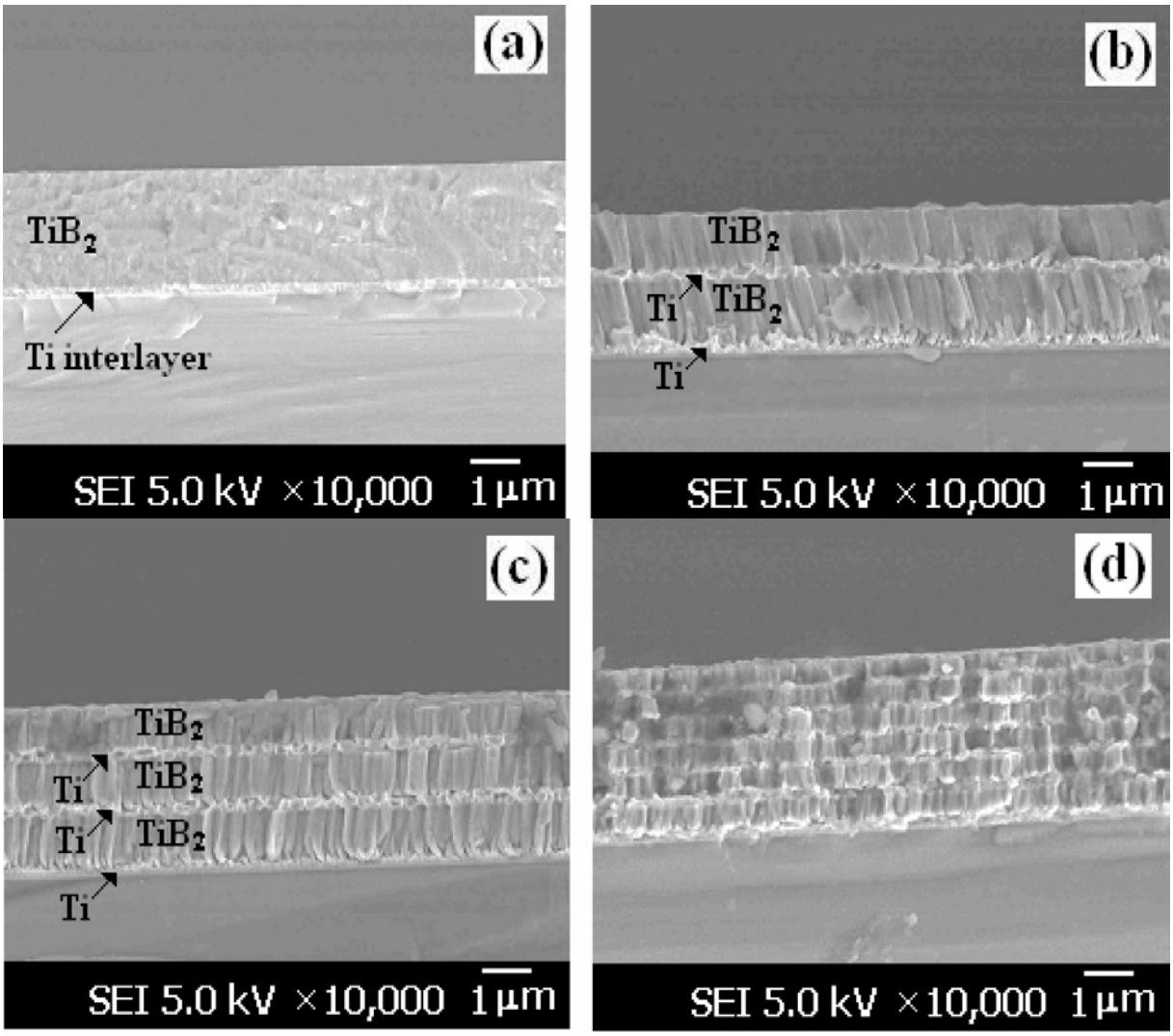

Fig. 3. FESEM images showing the fractured cross-section of (a) sample 1, (b) sample 2, (c) sample 3, and (d) sample 4.

3. RESULTS AND DISCUSSION

3.1. Structural characteristics

Fig. 2 shows the X-ray diffraction patterns recorded for the four coatings listed in Table 2. Each pattern shows several broad reflection peaks corresponding to the hexagonal TiB_2 structure. From Fig. 2, the peak (001) could be observed in all samples, in particular the graded layer (sample 1). Small peaks of Ti were also found from Ti interlayer for multilayer samples (samples 2-4) as expected. The broadness of the reflected peaks indicates the nanocrystalline nature of the coating structure, as further confirmed by FESEM examination (Fig. 3). For graded layer (sample 1), the presence of a single peak suggests a fiber texture with (001) preferred orientation of the specific crystal plane due to rich and thick TiB_2, which Ti underlined, could not be detected. However from Fig. 2, it is noted that the preferred (001) peak decreases with the increase of the alternate layers (decreasing TiB_2 layers) in particular, sample 4 (30 min TiB_2 coating on top), whilst the TiB_2 (100) peak increases with decreasing TiB_2 layers.

In addition, sample 2 (4 alternate Ti and TiB_2 layers) shows a small Ti (002) peak detected from Ti interlayer, which could be found significantly in sample 3 (6 alternate Ti and TiB_2 layers). The most interesting observation from Fig. 2 is that the multilayer Ti/TiB_2 coatings with depositing 6 alternate Ti and TiB_2 layers (sample 3) did not show any preferred orientation, whilst the graded layer (sample 1) and multilayer Ti/TiB_2 coatings with depositing 4 alternate Ti and TiB_2 layers (sample 2) showed a strong preferred (001) orientation, with the basal

Table 2. Conditions used in the tribological experiment.

Experiment	wear radius (mm)	applied normal load (N)
1	4	5
2	5	10

Table 3. Properties of resultant coatings.

Samples	Layers	Coating thickness (micron)	Average roughness, Ra (nm)	Hardness (GPa)	Reduced modulus (GPa)	Critical load Lc (mN)
No.1	2 layers	2.20	2.33	34.3 ± 1.2	329.5 ± 4.2	1,240
No.2	4 layers	2.52	15.49	33.4 ± 0.9	340.2 ± 5.2	1,855
No.3	6 layers	3.10	18.18	35.6 ± 2.2	365.4 ± 7.2	1,995
No.4	12 layers	3.42	20.61	20.1 ± 5.9	126.4 ± 9.5	1,650

plane parallel to the substrate surface. This may take account that TiB_2 coating needs more time to develop the preferred (001) direction, which only an hour of deposition time for TiB_2 is not enough (sample 3). Clearly, sample 4 in Fig. 2 shows a small peak of the preferred (001) direction due to the lack of time to develop the (001) peak as deposited TiB_2 for only 30 min.

Since TiB_2 coatings with (001) orientation is known to yield the highest hardness as compared with TiB_2 coatings with other orientation [12], it is believed that sample 1 with the highest (001) peak may show the highest hardness. In this study, however, the multilayer Ti/TiB_2 coatings with depositing 6 alternate Ti and TiB_2 layers (sample 3) shows the highest hardness value around 36 GPa despite showing a lower (001) peak compared to samples 1 and 2.

The fractured cross-sections of all samples were examined under FESEM, as shown in Fig. 3. It is obvious that the thin Ti interlayer could be observed in all samples. From Fig. 3, it can be seen that the multilayer coatings (samples 2-4) exhibit a columnar structure, which is typical of sputter deposition at relatively low adatom energies and limited mobility. This may be due to the incorporation of Ti interlayer. On the other hand, the graded layer coating (sample 1) exhibited a dense grain structure, obviously arising from the higher adatom energy.

From the above XRD and structural examinations, it is clear that with the more multilayer, TiB_2 coatings have the more random orientations and columnar structure, whilst the graded layer coating produced under the same conditions shows strong (001) orientation and dense grain structure. Actually, these strong (001) orientation and dense grain structure of graded layer can be explained by the effect of stationary substrate, which lies in the energy of the sputtered species arriving the substrate surface. It is known that the energy of the sputtered species decreases with increasing substrate-target distance due to increased collisions between the sputtered species and the gas molecules in the sputtering atmosphere [13-15]. The energy of the sputtered species arriving the stationary substrates is thus higher than that arriving the rotating substrates, and this would lead to increased adatom mobility and development of the (001) orientation and a denser structure in the coating. However in this study, for the multilayer cases, the adatom mobility and development of the preferred (001) orientation were obstructed by the Ti interlayer, which reduces the surface mobility of the adatom at the growing film surface resulted in the change of physical structure of coatings, such as columnar structure as shown in Fig. 3 (b), (c), and (d).

3.2. Tribological properties

By comparing Figs. 4 and 5, it can be observed that there are less fluctuation and scattering in Fig. 5. Through the evaluation of both figures, it can be noted that the curves under the 2 different loads, 5 and 10 N, were quite consistent. Moreover, the critical distances of the samples under the two loads are constant and this further proved the reliability

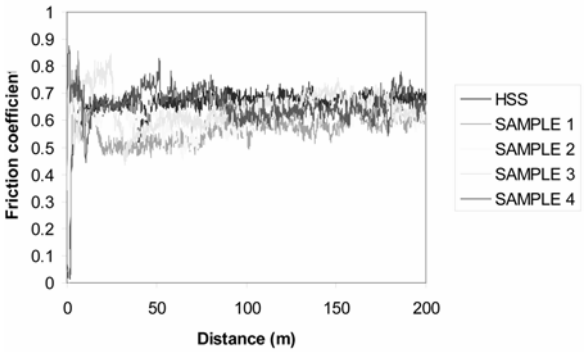

Fig. 4. Friction coefficient curves of the substrate and 4 samples loaded under 5 N.

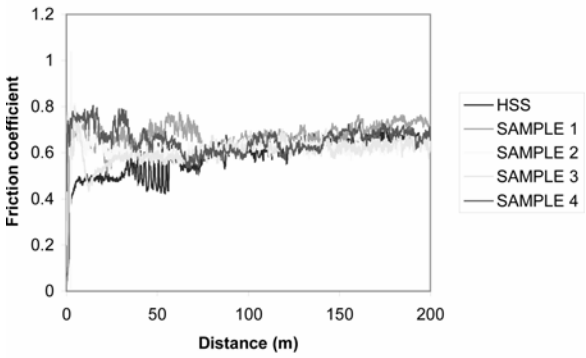

Fig. 5. Friction coefficient curves of the substrate and 4 samples loaded under 10 N.

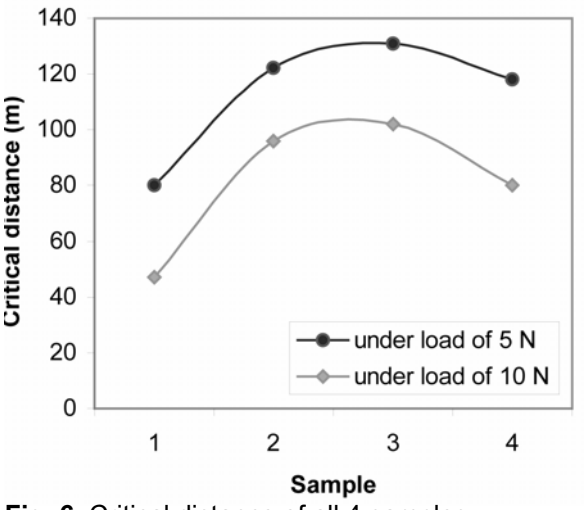

Fig. 6. Critical distance of all 4 samples.

and credibility of these wear tests. The critical distance, which is the approximated distance at which the friction coefficient of the curves reaches the point of stabilization (substrate) is evaluated and illustrated in Fig. 6.

It can be seen that sample 3 shows the longest critical distance in both types of experiments (loaded under 5 and 10 N). This indicates that coating of sample 3 took a longer time to reach the stable stage (substrate). Hence, this implies that the coating posses the wear resistance among the 4 samples. On the other hand, it can be observed that sample 1 took a shorter time than the other samples to wear out. This seems to signify that sample 1 shows the least wear resistant and this could be due to the poor adhesion between the coating and substrate. Besides this, it also can be due to the brittleness of the TiB_2 coating that it cannot adhere well to the Ti interlayer coating, resulting in its early flaking off from the substrate.

SEM images of samples 1 to 4 show circular wear tracks tested under applied load of 5 and 10 N (Fig. 7). It is noted that the worn surface produced by the alumina slider is microscopically smoother and is not so heavily scored. As the wear test proceeds, the original contact areas are enlarged and more asperities brought into the contact. During this process, the thickness of the tested coating in contact area is progressively reduced due to material loss. There is evidence that material loss from the coating is caused by polishing and abrasion actions of the hard Al_2O_3 ball. Abrasive grooves has been observed on the contact area of the TiB_2 coating

A close examination of sample 1 indicates the presence of cracks within the boundary of the wear track (Fig. 8). This seems to signify that the coating was undergone a much more severe plastic deformation than other samples. This phenomenon was not being observed in the other samples. This seems to indicate that sample 1 was less resistant to crack formation and propagation. This may be attributed to their brittle nature that allows stress to be concentrated on the contact area, giving rise to brittle failure, normally observed in pure TiB_2 coatings.

By taking into consideration of both experiments conducted under 2 different loads, it can be observed that the sample 3 had the lowest wear volume loss (Fig. 9). The result obtained seems to indicate that sample 3 had the greatest wear resistance among all 4 samples. This is correlated to the hardness of the coated samples where it can be seen that the higher hardness value, the lower wear volume loss. The results seem to suggest that the wear resistance of the coating is positively related to its hard-

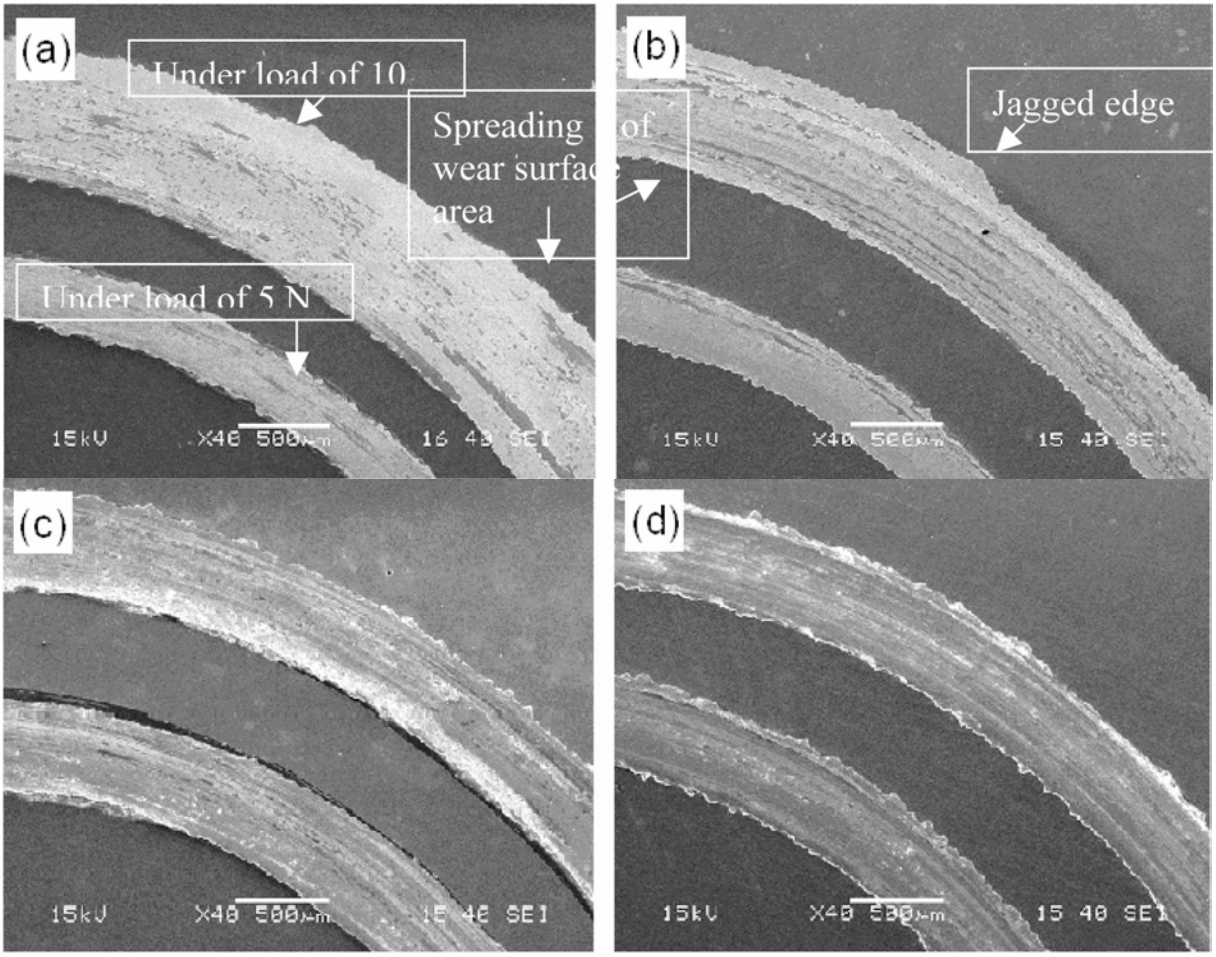

Fig. 7. SEM micrographs of the wear tracks of (a) sample 1, (b) sample 2, (c) sample 3 and (d) sample 4.

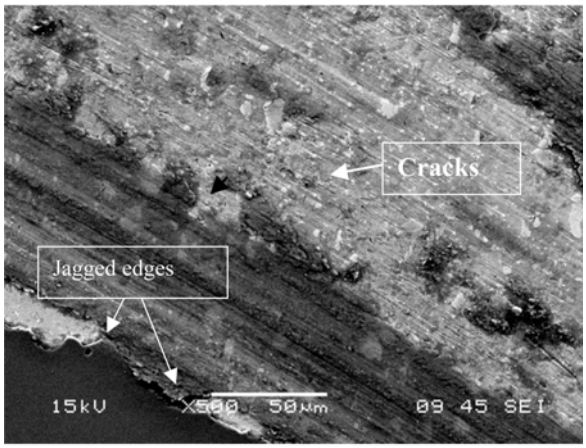

Fig. 8. Magnified micrograph of the wear track of sample 1, showing cracks and jagged edges.

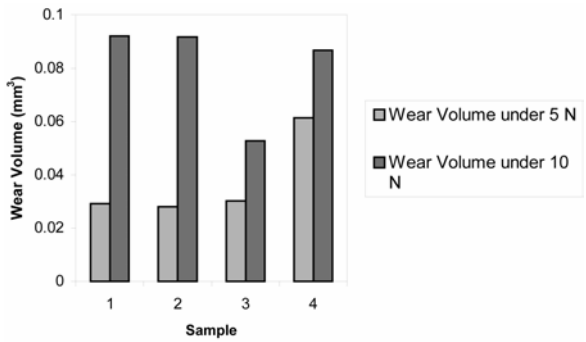

Fig. 9. Wear volume losses of all 4 samples.

ness value. It can also be observed the wear volume increases with increasing load applied. This is because the increasing load will increase the contact area between the alumina ball and the coating surface. Thus more materials would be pulled off as the alumina ball slide over the surface, leading to more adhesive wear of the coating.

From Fig. 9, the large wear volume loss of samples 1 and 2 could be due to the brittleness and poor adhesion of the coatings. This may be further confirmed by microscopic examination of the wear tracks as shown in Fig. 7. It can be seen that there was a wide spread of worn out surface area whereby the surrounding surface area of the wear track was also worn out. The poor adhesiveness of the coatings may aggravate the volume and rate of wear loss as the coatings had the tendency to flake more easily.

4. CONCLUSIONS

(1) From the experimental results, it can be concluded that under the present deposition conditions, magnetron sputtering of Ti and TiB_2 can be used to produce multilayer coatings with increased coating adhesion and relatively high hardness.

(2) It was found that the 6-layer coating gave the best results in terms of coating hardness and adhesion strength. This is due to the existence of an optimum combination of alternate layers that gives the optimal enhancement in coating adhesion.

(3) Under unlubricated sliding against an alumina ball, the TiB_2 based coatings produced under various deposition conditions increases the wear resistance of high speed steel. It is noted that all samples can improve the wear resistance of HSS. The TiB_2 based coating provides a hard layer to resist plastic deformation and eliminate adhesion between the test surface and the ball slider, which are the main reasons of severe wear of untreated HSS.

REFERENCES

[1] E. Matrubara, Y. Waseda, S. Takeda and Y. Taga // *Thin Solid Films* **186** (1984) L33.

[2] B. Todorovic, T. Jokic, Z. Rakocevic, Z. Markovic, B. Gakovic and T. Nanadovic // *Thin Solid Films* **300** (1997) 272.

[3] M. Berger // *Surface Engineering* **18** (2002) 219.

[4] J. Chen and J. A. Barnard // *Materials Science and Engineering A* **191** (1995) 233.

[5] R. Wiedemann, H. Oettel and M. Jerenz // *Surface Coatings and Technology* **97** (1997) 313.

[6] E. Kelesoglu and C. Mitterer // *Surface Coatings and Technology* **98** (1998) 1483.

[7] M. Berger, E. Coronel and E. Olsson // *Surface Coatings and Technology* **185** (2004) 240.

[8] M. Berger and M. Larsson // *Surface Engineering* **16** (2000) 122.

[9] J. P. Schlomka, M. Tolan, L. Schwalowsky, O.H. Seeck, J. Stettner and W. Press // *Physics Review B* **51** (1995) 2311.

[10] H. Zabel // *Applied Physics A* **58** (1999) 159.

[11] W. C. Oliver and G. M. Pharr // *Journal of Materials Research* **7** (1992) 1564.

[12] H. Holleck // *Journal of Vacuum Science and Technology A* **4** (1986) 2661.

[13] Waba Kiyotaka, *Handbook of sputter deposition technology: principles, technology, and applications* (Noyes Publications, Park Ridge, N.J. U.S.A., 1992)

[14] N. Panich and Y. Sun // *Thin Solid Films* **500** (2006) 190.

[15] N. Panich, P. Wangyao, N. Vattanaprateep and Y. Sun // *Journal of Metals, Materials and Minerals* **16/2** (2006) 19.